Waste Disposal & Sustainable Energy (2022) 4:283–295
https://doi.org/10.1007/s42768-022-00113-3

ARTICLE

Valorisation of alum sludge to produce green and durable mortar

Qiong Jia[1,2] · Yan Zhuge[1] · Weiwei Duan[1] · Yue Liu[1] · Jing Yang[2] · Osama Youssf[1,3] · Jinsuo Lu[2]

Received: 21 July 2022 / Revised: 19 August 2022 / Accepted: 6 September 2022 / Published online: 15 October 2022

Abstract

Alum sludge is a typical by-product of drinking water treatment processes. Most sludge is disposed of at landfill sites, and such a disposal method may cause significant environmental concern due to its vast amount. This paper assessed the feasibility of reusing sludge as a supplementary cementitious material, which could efficiently exhaust stockpiled sludge. Specifically, the pozzolanic reactivity of sludge at different temperatures, the reaction mechanism of the sludge–cement binder, and the resistance of sludge-derived mortar to microbially induced corrosion were investigated. The obtained results indicated that 800 °C was the optimal calcination temperature for sludge. Mortar containing sludge up to 30% by weight showed comparable physical properties at a curing age of 90 days. Mortar with 10% cement replaced by sludge can significantly improve the resistance to biogenic corrosion due to the formation of Al-bearing phases with high resistance to acidic media, e.g., $Ca_4Al_2O_7{\cdot}xH_2O$ and strätlingite.

Graphical abstract

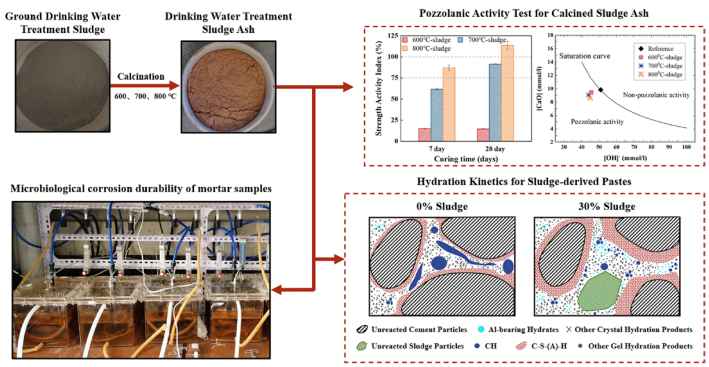

Keywords Alum sludge · Pozzolanic activity · Microbially induced corrosion · Cement-based composites · Utilisation of waste

Introduction

Alum sludge is a typical by-product of the water industry. When the aluminium-based coagulant was combined with suspended solids, dissolved colloids, organic matter, and microorganisms in raw water, the heterogeneous solid waste was formed [1, 2]. At the current stage, the domestic and industrial water demand has increased dramatically due to the rapid growth of the global population, economic development, and changes in the consumption structure, resulting in large quantities of sludge [3, 4]. It is estimated that the daily production of sludge has exceeded

✉ Yan Zhuge
Yan.Zhuge@unisa.edu.au

✉ Jinsuo Lu
lujinsuo@xauat.edu.cn

1 UniSA STEM, University of South Australia, Adelaide, SA 5000, Australia

2 School of Environmental and Municipal Engineering Department, Xi'an University of Architecture and Technology, Xi'an 710055, China

3 Structural Engineering Department, Faculty of Engineering, Mansoura University, Mansoura 35516, Egypt

10,000 t globally [5]. Sludge is commonly disposed of in landfills. Since most of the sludge has not been treated innocuously, sludge landfilling causes severe environmental issues related to land wastage and secondary pollution. For instance, some sludge is rich in pathogens and metals (e.g., Al, Cu, and Fe), and the leaching of aluminium into surrounding water may indirectly result in an increase in aluminium concentration in the human body, contributing to the occurrence of Alzheimer's disease [6]. In addition, some toxic heavy metals, e.g., Pb, As, and Cr, present in sludge may cause potential risks when sludge is exposed to aquatic environments [7]. Therefore, managing sludge in a more economical and environmentally friendly manner is required.

Alum sludge has been reused in various sustainable options, e.g., as a source for recovery of coagulants, as a contaminant absorbent for wastewater treatment, and as a raw material for ceramic production, constructing wetland substrate, or soil ameliorant [8]. In recent years, some studies focused on assessing the feasibility of reusing alum sludge as supplementary cementitious material in concrete products, proposing a possible solution to reuse sludge in large quantities. In addition, reusing sludge as cement replacement contributes to reducing cement-derived CO_2 emissions (about 8% of global CO_2 emissions) [9], which helps to achieve net-zero emissions by 2050.

The pozzolanic reactivity of sludge can be activated with designed calcination and grinding procedures. Gastaldini et al. [10] suggested that the optimum treatment procedure for sludge was calcination at 600 °C for 1 h. The obtained compressive strength of sludge-derived concrete was comparable to the reference values. Tantawy [11] reported that the calcination of sludge at 800 °C preserved the optimal pozzolanic activity, and the partially crystal phases of silicon and aluminium were dehydroxylated to form high reactivity disordered phases between 600 °C and 800 °C. However, higher temperatures, such as 900 °C, might cause the re-formation of crystal silica phases in sludge. Hagemann et al. [12] suggested that calcination at 700 °C with a residence time of 1 h was the best condition for treating sludge. Therefore, controversy still exists over the optimum treatment conditions for sludge.

On the other hand, microbially induced corrosion (MIC) is regarded as one of the main deterioration mechanisms to reduce the service life of concrete structures exposed to sewer environments [13]. Sulphate-reducing bacteria (SRB) could produce hydrogen sulphide (H_2S) by reducing sulphate in sewage, which is in turn used as a nutrient by sulphur-oxidising bacteria (SOB), resulting in the formation of sulphuric acid (H_2SO_4) [14]. The H_2SO_4 generated through the biological metabolism reacts with the cement hydration phases, such as calcium hydroxide (CH) and calcium silicate hydrate (C–S–H), to form gypsum and ettringite, leading to the expansion and progressive disintegration of concrete structure [15]. However, Scrivener et al. [16] found that aluminium-rich hydration products exhibited superior resistance to BSA (biogenic sulfuric acid). Also, Saucier et al. [17] reported that the aluminium-bearing hydrates could dissociate to alumina gel under acidic conditions, which formed an acid-resistant barrier to slow down the biogenic sulfuric acid diffusion. Moreover, the further dissolution of alumina gel liberated the aluminium ions, which inhibited the bacteria from producing sulfuric acid and stopped pH decreasing. Alum sludge contains a high volume of reactive aluminium, which promotes the formation of aluminium-bearing hydrates, such as calcium aluminate hydrate (C–A–H) [18, 19]. Therefore, the cement-based composites incorporating sludge may improve the resistance to MIC, and there is no available literature in this area.

This study aims to: (i) characterise the pozzolanic reactivity of sludge under different calcination temperatures and investigate the reaction mechanism of blended binder; (ii) evaluate the setting times, workability, and compressive strength of sludge-derived mortar; (iii) assess the resistance of mortar to MIC in terms of mass loss and corrosion depth.

Materials and methodology

Materials

A general-purpose (GP) cement, based on AS 3972 [20], was used in this study. Alum sludge was obtained from a local water treatment plant in South Australia. Raw alum sludge contained approximately 29.5% organic matter content, which was determined based on the loss on ignition (LOI) test according to ASTM D7348 (2013) [21]. The chemical composition of the raw sludge is shown in Table S1, referring to a previous study conducted by the authors. The major components of sludge were Al_2O_3, SiO_2, and organic matter. Minor constituents of Fe_2O_3, CaO, K_2O, and MgO were also observed. Figure S1 shows the scanning electron microscopy (SEM) images of sludge, exhibiting an irregular shape and porous structure of sludge particles.

Raw alum sludge was first oven-dried at 105 °C for 24 h. The dried sludge was then ground in a ring mill until the size was less than 75 μm. The calcination of sludge was conducted in a muffle furnace. To compare the pozzolanic reactivity of sludge under different temperatures, the furnace was programmed with peak temperatures of 600 °C, 700 °C, and 800 °C for 2 h, respectively. Silica

sand was used as fine aggregates, and sand properties are shown in Table S2.

The chemical composition of cement and the calcined sludge was obtained by x-ray fluorescence analysis using S4 PIONEER spectrometer (Bruker AXS GmbH, Karlsruhe, Germany). As the chemical composition of sludge calcinated at 600 °C, 700 °C, and 800 °C was similar; only the 800 °C treated sludge was shown. The particle size distribution and Blaine fineness of binder materials were determined using a laser diffraction particle analyzer (Malvern Mastersizer 3000, Malvern PANalytical Ltd, Malvern, UK). The specific gravity and water absorption of sludge were identified based on AS 1141.5 [22]. Moreover, sludge morphology was identified using SEM by Carl Zeiss Microscopy Crossbeam 540 with GEMINI II column (Jena, Germany). The mineralogical characterisation of sludge before and after calcination was conducted using an Empyrean diffractometer (Malvern PANalytical, Malvern, UK). The scanning angle ranged from 5° to 70° (2θ).

Pozzolanic activity

The pozzolanic activity of sludge under different heating temperatures was assessed using the Strength Activity Index (SAI) test and the Frattini test. SAI test was conducted based on ASTM C311 [23]. The SAI was calculated with Eq. (1), where A is the average compressive strength of mortar with 20% cement replaced by sludge, and B is the average compressive strength of the reference ones (without sludge). Also, SAI greater than 0.75 indicates a satisfying pozzolanic activity.

$$\mathrm{SAI} = \frac{A}{B} \times 100\% \,. \tag{1}$$

The Frattini test was performed according to BS EN 196-5 [24]. A 20 g sample was prepared with 80% cement and 20% sludge mixed with 100 mL water. The mixture was stored in a controlled oven at 40 °C for 15 days with a sealed polyethylene container. The samples were then immediately filtered into the vacuum flask using a dry double filter paper and cooled down to room temperature. Hydrochloric acid titration with methyl orange indicator was used to determine the hydroxide [OH^-] concentration in the filtrate. After adjusting the solution's pH to 12.5, the concentration of calcium ions [Ca^{2+}] was analysed by titration using a 0.03 mol/L EDTA solution with the Murexide indicator. The obtained results were compared with the solubility curve of CH. The solubility curve was determined on Eq. (2) according to BS EN 196-5 [24], indicating the theoretical maximum [CaO] concentration with a given [OH^-] value. Points plotted according to [Ca^{2+}] and [OH^-] concentration below the solubility curve indicated a positive pozzolanic reactivity of sludge.

$$\mathrm{Max[CaO]} = \frac{350}{[\mathrm{OH}^-] - 15}. \tag{2}$$

Sample preparation

The mixed proportion of the binder pastes and mortars in this study is shown in Table 1. Sludge was used as a supplementary cementitious material to replace 10%, 20%, and 30% of cement by weight in both binder pastes and mortar specimens. Mortar mixing was conducted based on ASTM C305 [25], and the mixing of pastes followed the same procedure but without fine aggregates. A polycarboxylate-based superplasticizer was added to maintain constant relative flowability. The required superplasticizer amount increased with increasing sludge content due to the high water absorption of sludge, as confirmed in a previous study [26]. The fresh mortar mixtures were cast into molds with 50 mm × 50 mm × 50 mm, and the fresh binder pastes were cast into molds with 10 mm × 10 mm × 10 mm. The samples were de-molded after 24 h and then cured in a moist chamber with a constant temperature of 23±2 °C and a constant relative humidity of 95%.

Tests

Physical properties of mortar

The setting time of fresh binder pastes under standard consistency was determined with the Vicat apparatus according to BS EN 196-3 [27]. The fluidity test of the fresh mortar pastes was conducted according to BS EN 1015-3 [28]. All tests for mortar samples were conducted with at least three samples, and average values with standard deviations were reported. The compressive strength of mortar samples was measured at curing ages of 7 d, 28 d, and 90 d based on AS 1012.9 [29].

Table 1 Mix proportions of the binder pastes and mortars (kg/m^3)

Mix	Sludge	Cement	Water	Sand	SP
Binder paste					
BP-0	0	1219	590	0	3.66
BP-10	122	1097	590	0	6.10
BP-20	244	975	590	0	8.53
BP-30	366	853	590	0	12.19
Mortar					
M-0	0	620	300	1705	1.86
M-10	62	558	300	1705	3.10
M-20	124	496	300	1705	4.34
M-30	186	434	300	1705	6.20

SP superplasticizer, *M* mortar, *BP* binder paste

The water capillary absorption tests were conducted according to ASTM C1585 [30]. The mortar specimens cured for 90 d were first oven-dried at 50 °C until constant weight. The lateral sides of samples were then sealed with an epoxy resin, and the water level was kept at 3 mm above the submerged surface with an open area of 50 mm × 50 mm. Weight measurements were conducted at 0 s, 60 s, 300 s, 600 s, 1200 s, 3600 s, 7200 s, and 21600 s, and daily measures were subsequently taken for the next 8 d using a balance with an accuracy of ±0.01 g. The amount of water that penetrated per unit area was calculated based on Eq. (3), where I is the absorption (mm); m_t is the mass change (g) at time t (s); a is the open area (mm^2); d refers to the density of water (g/mm^3).

$$I = \frac{m_t}{a \times d}. \tag{3}$$

For mass loss measurement, mortar samples were first brushed to remove the soft particles and then oven-dried at 40 °C until constant weight. The weight of specimens before and after soaking was measured using a balance with an accuracy of ± 0.01 g. The mass loss of mortar samples was calculated by Eq. (4).

$$m\% = \frac{m_t - m_o}{m_o} \times 100\% \,. \tag{4}$$

Phenolphthalein reagent was used to indicate the corrosion depth of specimens. Corroded samples were dry-cut along the cross-section, and the cut surface was then sprayed with 1% phenolphthalein alcohol solution. The vertical distance between the boundary of the colourless area and the mortar surface indicated the corrosion depth. The results were averaged over five measurements.

Microbiological corrosion durability

Thiobacillus ferrooxidans (T. f) was used as the SOB to activate the MIC on mortar. T. f was cultured in the 9 K medium, in which the components were 1000 mL H_2O, 3 g $(NH_4)_2SO_4$, 0.1 g KCl, 0.5 g K_2HPO_4, 0.5 g $MgSO_4{\cdot}7H_2O$, 0.01 g $Ca(NO_3)_2$, and 44.78 g $FeSO_4{\cdot}7H_2O$. As shown in Fig. 1, the sealed corrosion chamber was kept at 30 °C. Gaseous H_2S and air were aerated into the bacteria liquid to provide reducing substances and appropriate aerobic conditions for T. f to generate sulfuric acid. Mass loss and corrosion depth of the mortars were measured to evaluate the degree of corrosion when the specimens were soaked in bacteria corrosive medium for 2 months.

Microstructural characterizations

The crystalline phases of binder pastes were determined by X-ray diffractometry (XRD), which was conducted by an Empyrean diffractometer (Malvern PANalytical, Malvern, UK) with Cu Kα radiation. Before the test, binder pastes were crushed to less than 36 μm. The hydration reaction of blended binders was stopped by immersing samples in the ethanol solution for two days and then vacuum dried at 40 °C until constant weight. The compound composition of binder pastes was investigated by thermogravimetric analysis (TGA) using the Discovery 650 DSC/TGA machine. Powdered samples were placed in a 150 μL crucible and heated from 50 °C to 1000 °C at a rate of 10 °C/min with N_2

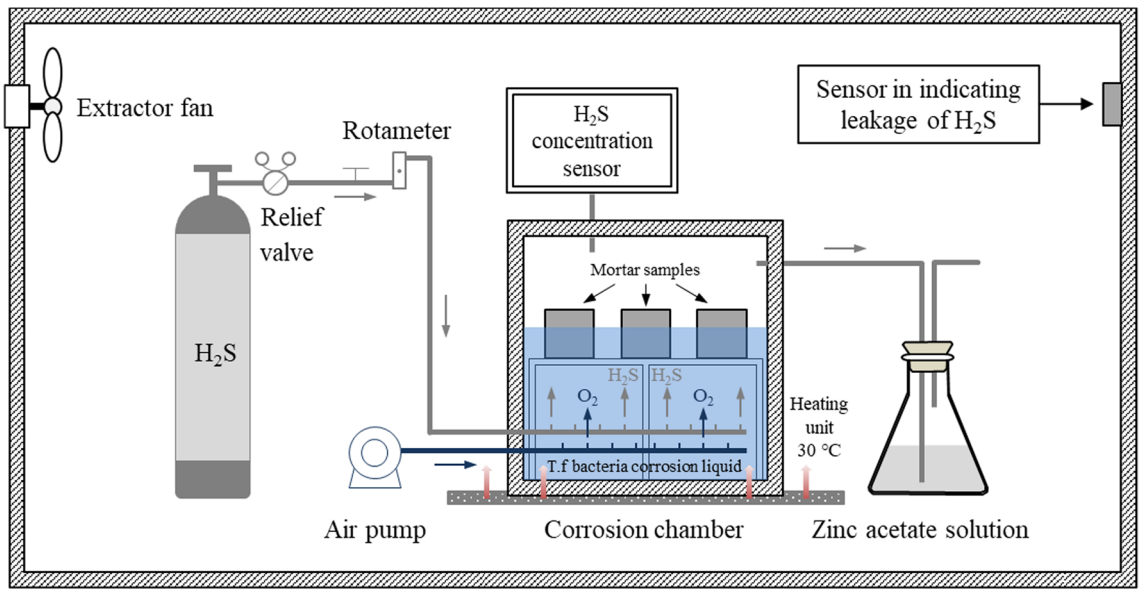

Fig. 1 Schematic diagram of MIC corrosion test. *MIC* microbially induced corrosion

Table 2 Properties of binder materials

Chemical composition				
Oxide	Percentage by mass (%)		Chemical requirements of natural pozzolans based on ASTM C618 [32]	
	GP cement	Calcined sludge		
SiO_2	20.8	31.1	$SiO_2 + Al_2O_3 + Fe_2O_3 \geq 70\%$	
Al_2O_3	3.6	47.7		
Fe_2O_3	4.0	4.9		
CaO	61.8	4.3	–	
CuO	–	0.3	–	
K_2O	0.8	1.0	–	
MgO	2.7	1.0	–	
Na_2O	0.1	0.2	–	
SO_3	2.7	3.0	$\leq 3.0\%$	
LOI	3.3	6.6	$\leq 10.0\%$	
Physical properties	Cement	600 °C sludge	700 °C sludge	800 °C sludge
D10 (μm)	3.4	5.4	5.8	6.1
D50 (μm)	14.5	29.6	29.2	30.4
D90 (μm)	33.1	61.3	60.3	60.9
Blaine fineness (m^2/kg)	400.0	445.4	429.8	423.4

DX The portion of particles with diameters smaller than this value is X%, *GP* general-purpose

as purging gas. The microstructural morphology of mortar samples was investigated with SEM images, which were obtained with Carl Zeiss Microscopy Crossbeam 540 with the GEMINI II column (Jena, Germany). In addition, the local morphology of the corroded mortar interface was also characterised.

Results and discussion

Chemical composition and pozzolanic activity of sludge

The chemical composition and physical properties of cement and calcined sludge are shown in Table 2. Sludge calcined at different temperatures exhibited a similar particle size distribution, and the D50 value was around 30 μm, which was coarser than that of cement particles (14.5 μm). However, the Blaine fineness of sludge was generally comparable to or even higher than that of cement clinker. These results can be attributed to the fact that sludge has an irregular shape with a porous surface texture, which is confirmed by the SEM image (see Fig. 2a). Meanwhile, such a porous structure resulted in high water absorption of sludge (15.3%) and low specific gravity (2.2). The Blaine fineness of sludge decreased with increasing calcination temperatures. These results were consistent with previous results reported by Fabbri et al. [31], which found that the dehydroxylated fine particles always agglomerated under high temperatures to produce new porous grains. In addition, calcined sludge contains a higher aluminium content than cement, with a mass proportion of 47.7%. The components of Al_2O_3, SiO_2 (31.1%), and Fe_2O_3 (4.9%) add up to greater than 70%. Also, the content of SO_3 and the LOI were 3.0% and 6.6%, respectively. These results indicate that the chemical composition of treated sludge conforms to the requirements of natural pozzolan material prescribed in ASTM C618 [32]. The mineralogical composition of sludge under different calcination temperatures is shown in Fig. 2b. The results indicated that the crystalline content of raw sludge was dominated by quartz, kaolinite, and aluminium sulphate hydroxide hydrate. Also, low amounts of calcite, albite, and lizardite were present. The evolution of XRD patterns with increasing temperatures indicated a significant loss of kaolinite, and the peaks corresponding to kaolinite diminished at 600 °C until they completely disappeared at 800 °C. Moreover, the calcite ($CaCO_3$) collapse occurred at 600 °C, and the formation of new crystalline phases such as calcium sulphate and microcline were observed simultaneously. A peak of crystalline aluminium sulphate hydroxide hydrate (2θ=19.8°) decreased with increasing calcination temperature, indicating the transformation into amorphous aluminium-containing phases, which may present high reactivity compared with the crystalline one. Also, no significant change was observed for inert minerals such as quartz, albite, and lizardite. Therefore,

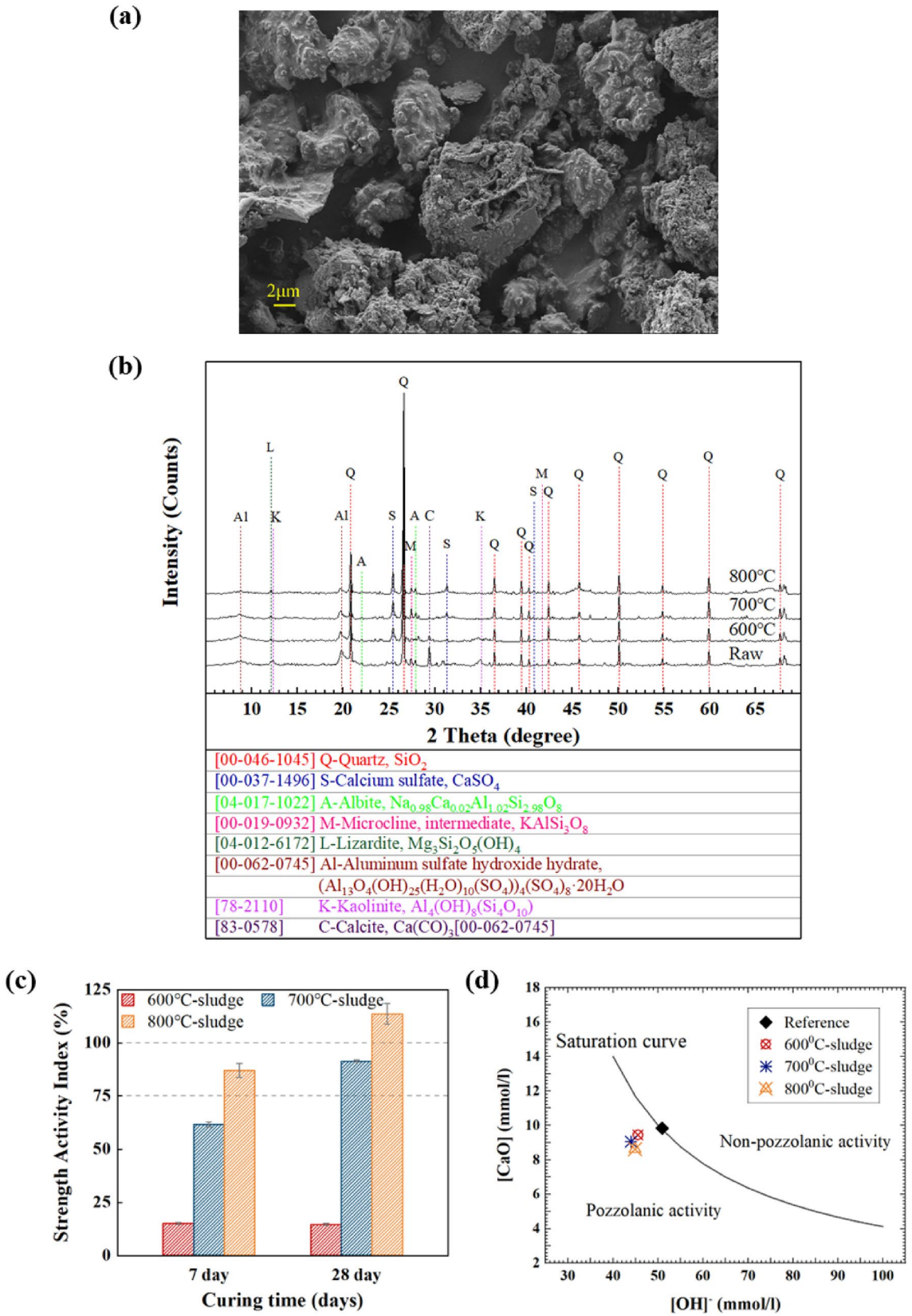

Fig. 2 (**a**) SEM image of sludge calcinated at 800 °C; (**b**) XRD patterns of sludge treated with different temperatures; (**c**) strength activity index at curing ages of 7 and 28 days; (**d**) Frattini test results. *SEM* scanning electron microscopy, *XRD* X-ray diffractometry

Table 3 Quantified results of the Frattini test

Sludge	$[OH^-]$ (mmol/L)	[CaO] (mmol/L)	Max [CaO] (mmol/L)	[CaO] reduction %
600 °C	45.5	9.5	11.5	17.5
700 °C	44.0	9.1	12.1	25.1
800 °C	44.9	8.6	11.7	26.4

the XRD analysis exhibits that more aluminium-containing amorphous phases with high reactivity may be present in the 800 °C sludge due to the completed dehydroxylation of kaolinite and continued phase transition of aluminium sulphate hydroxide hydrate.

SAI and Frattini tests were used to further study the pozzolanic activity of sludge. As shown in Fig. 2c, the mortar samples containing 600 °C sludge exhibited significantly low SAI values at curing ages of 7 d and 28 d. When the calcination temperature increased to 700 °C, the mortar samples at a curing age of 28 d exhibited a satisfactory SAI value, which was above 75% (prescribed in ASTM C618 [32]). The samples containing 800 °C sludge showed the highest pozzolanic activity at all curing ages, and the SAI was 87% at 7 d and 114% at 28 d. Besides, the results of the Frattini test (see Fig. 2d) indicated that sludge calcined at 600 °C, 700 °C, and 800 °C all showed pozzolanic activity after 15 d.

To further compare the pozzolanic activity of sludge calcined at different temperatures, the Frattini test results were quantified as suggested by Donatello et al. [33]. Theoretical maximum [CaO] was calculated using Eq. (2). The difference between [CaO] concentration and theoretical Max [CaO] is expressed as the reduction percentage of the [CaO]; the calculated results are shown in Table 3. The results exhibited that the reduction percentage of [CaO] increased with increasing calcination temperatures, indicating that the pozzolanic reactivity of sludge increased with increasing calcination temperature. These results were consistent with the XRD results. Combined with the SAI and Frattini test results, 800 °C is the optimum temperature to activate the pozzolanic reactivity of sludge. Therefore, all mortar and binder paste samples were prepared with sludge calcinated at 800 °C.

Table 4 Fresh properties of binder pastes

Mix	W. content [g]	Consistency [mm]	Initial set [min]	Final set [min]
Control	142	6.8	111	166
BP-10	169	6.1	177	224
BP-20	197	6.8	140	190
BP-30	225	6.5	65	92

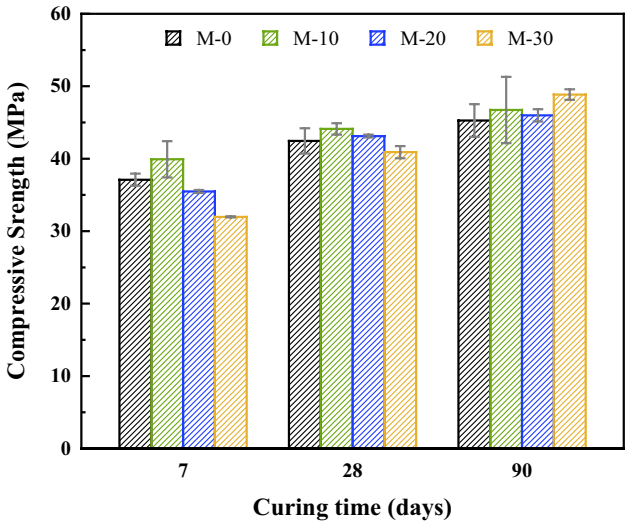

Fig. 3 Compressive strength of mortar samples

Physical properties of sludge-based composites

The measured flow values of fresh mortar pastes are given in Fig. S2. The fluidity decreased from 187 mm to 142 mm with increasing sludge content from 0 to 30%. In addition to the large surface area of sludge, the irregular morphology of sludge also harms flowability. According to Shi et al. [34], sludge particles with varying sizes caused mechanical inter-lock between each other, and a considerable space between them could detain the mixing water, decreasing the flowability of fresh mortar mixture. Also, binder pastes containing sludge required more mixing water to maintain standard consistency. As shown in Table 4, the sludge addition substantially increased the water demand for pastes, especially for the samples containing 30% sludge.

For the setting time of binder pastes (see Table 4), the setting time was significantly retarded compared to the reference mix when 10% cement was replaced with sludge. However, the setting time was gradually reduced with a further increase in sludge content. These results indicated that sludge addition could affect the setting time from two opposite aspects. On the one hand, the incorporation of sludge increases the water demand, resulting in the delay of setting. On the other hand, the amorphous aluminium phase in the calcined sludge reacts faster than calcium silicate clinkers, leading to shorter initial and final setting times. Meanwhile, sludge may have a filler effect, providing additional nucleation sites to accelerate cement hydration [16]. Alum sludge seemed to have different effects on setting time depending on the percentage used in the binder. A further study on the hydration behaviour of sludge-cement binder is required to explain such setting behaviour in detail.

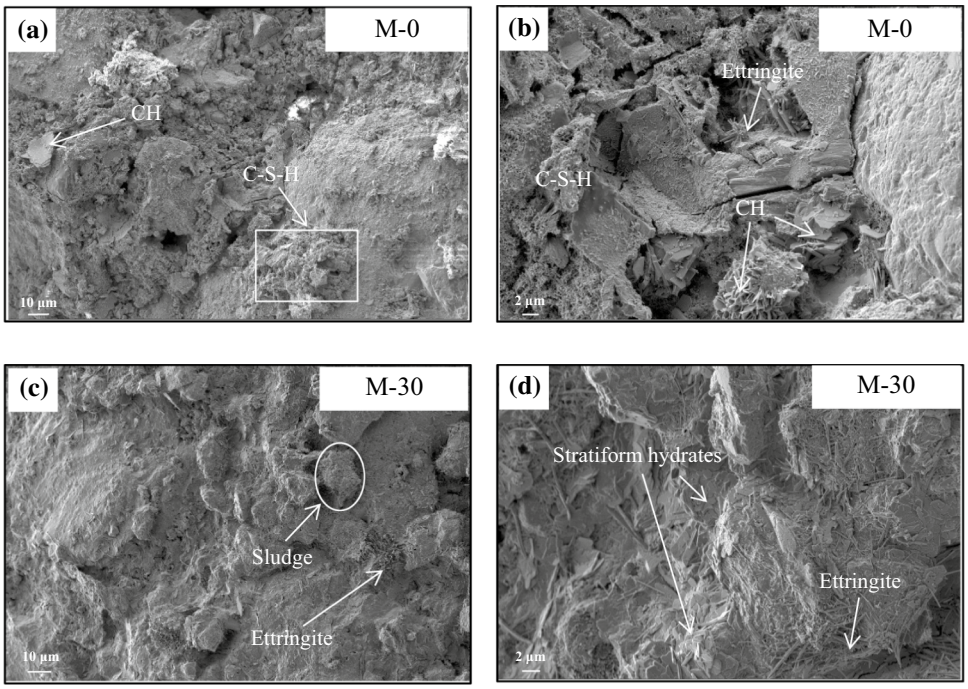

Fig. 4 SEM images of mortar (**a**) and (**b**) 0 sludge, (**c**) and (**d**) 30% sludge

The effects of sludge addition on the compressive strength of mortar samples are shown in Fig. 3. Compared to the reference samples, 10% sludge addition exhibited a higher compressive strength after curing for 7 days, resulting from the filler effect (confirmed by thermal analysis in Section "Hydration kinetics"). The strength of the samples containing 20% and 30% sludge decreased with increasing sludge content and showed a lower compressive strength than the reference ones at 7 d. Such a strength reduction indicated that the cement dilution effect dominated the reaction mechanism at an early curing age, especially for M-30. As the hydration continued, the strength of mortar with higher sludge content increased noticeably. At a curing age of 90 d, the samples with 30% sludge exhibited the highest compressive strength. These results were attributed to the fact that the pozzolanic reaction of sludge prevailed at later curing ages; the cement dilution effect in the samples with 30% sludge was completely compensated at 90 d.

SEM results confirmed the occurrence of the pozzolanic reaction. Figure 4 illustrates the SEM images of the mortar samples containing 0 and 30% sludge at a curing age of 90 d. In Fig. 4a, the cotton-shaped C-(A)–S–H gel was observed, and some crystals with a hexagonal plate morphology were visible, indicating the presence of CH. Also, the needle-shaped ettringite is shown. Compared with the reference samples, a large amount of crystalline ettringite stockpiled on the surface of samples containing 30% sludge (see Fig. 4b). The CH with hexagonal plate clusters was rarely seen in M-30 because of the consumption by the pozzolanic reaction. Instead, many stratiform hydrates were observed. Combined with the XRD analysis in Section "Hydration kinetics", these laminar phases might correspond to the presence of $Ca_4Al_2O_7{\cdot}xH_2O$ and strätlingite, which were derived from the pozzolanic reaction of sludge. These hydration products help to achieve higher mechanical strength at later ages of the mortar samples.

The water capillary absorption of mortar samples containing sludge is shown in Fig. 5. The results showed that the sorptivity of specimens containing sludge was higher than that of the control one. These results suggested that the cement matrix incorporating sludge might exhibit higher total porosity than the reference ones. However, the pores were refined due to the secondary pozzolanic reaction. Such a finer pore system increased the sorptivity but showed little correlation with strength [35, 36]. Also, the higher water absorption of sludge contributed to the amount of total water absorbed by mortar samples, which was an adverse factor for durability.

Hydration kinetics

The TGA and DTG curves of mortar samples are shown in Fig. S3. As shown in Fig. S3, the intensity of the endothermic peak at 400–500 °C corresponds to the decomposition of CH, and the CH amount of cement can directly reflect the degree of pozzolanic reaction [37]. Figure 6 shows the CH amount of binder pastes at 7 d, 28 d, and 90 d. The straight dotted line (normalised CH content) represents the amount of CH in the pure cement paste mixture multiplied by the cement content ratio. The difference between the measured data and the straight line indicates the consumption of CH

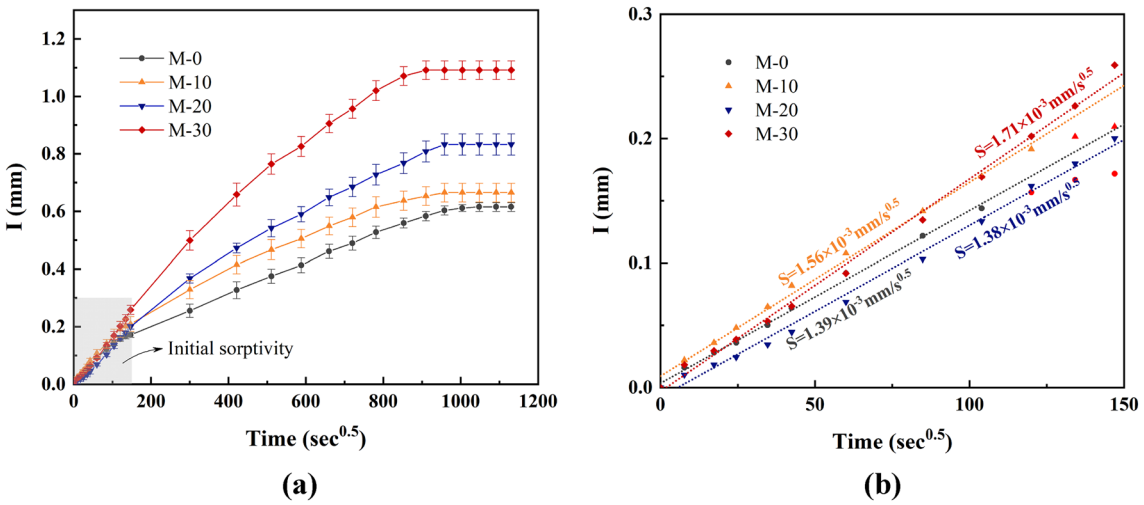

Fig. 5 The absorption and sorptivity characteristics of mortar samples. (**a**) Capillary water absorption, (**b**) initial sorptivity

by the pozzolanic reaction. At 7 d, the paste samples with 10% and 20% sludge exhibited a higher CH content than the normalised samples, resulting from the filler effect. Only the samples with 30% sludge exhibited a moderate consumption of CH. After 28 d of curing, the CH amount of samples with 20% sludge was comparable to the normalised amount, indicating that the filler effect (promoting CH formation) and pozzolanic reaction (consuming CH) achieved a balance. The difference in CH amount between the normalised line and the samples containing 30% sludge continued to expand, and such CH consumption became more significant at a curing age of 90 d. At 90 d, the samples with 10% sludge exhibited a minor pozzolanic reaction, and the amount of consumed CH increased with increasing sludge content.

Generally, the reaction mechanism of mortar samples containing varying sludge content was not uniform. The samples containing 10% sludge exhibited a superior filler effect before 28 d, and the signal of pozzolanic reaction was evident at a curing age of 90 d. For the samples containing 20% and 30% sludge, pozzolanic behaviour was observed at early ages compared with the pastes containing 10% sludge. The pozzolanic reaction was pronounced in samples with

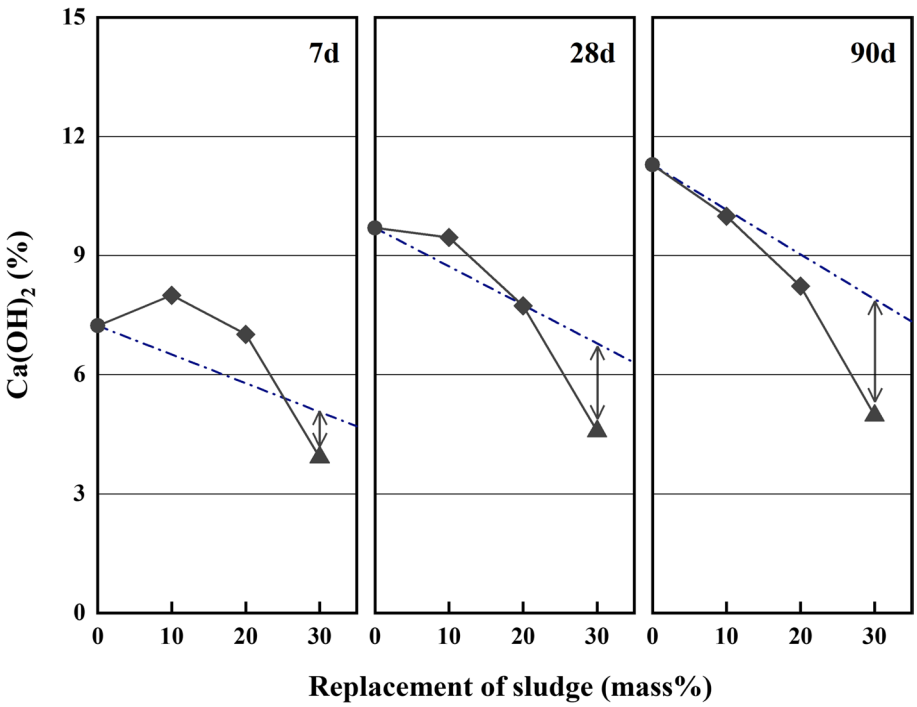

Fig. 6 Relation between the amounts of CH and the content of sludge in binder pastes

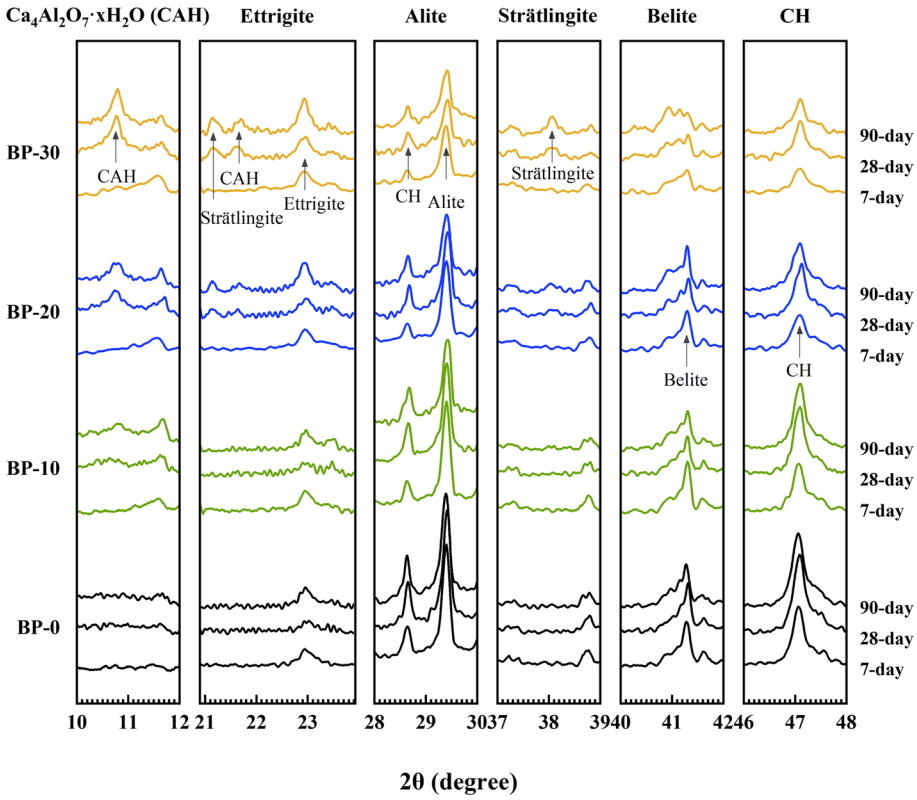

Fig. 7 XRD patterns of binder pastes at 7 d, 28 d, and 90 d

30% sludge. These results could be explained by the fact a large amount of reactive Al derived from sludge may accelerate the overall reaction rate, and the pozzolanic reaction happens before 7 d. Compared with fly ash, which starts to react even after 28 d [38], the pozzolanic reactivity of alum sludge is promising. These results were not consistent with a previous study, which reported that the samples with 10% sludge exhibited the highest degree of pozzolanic reaction [26, 39]. This may be attributed to the different mixture designs, such as the water-to-binder ratio.

XRD was conducted to further analyse the evolution of hydration products in the sludge-containing binder pastes with pozzolanic reactions. As shown in Fig. 7, the main crystalline hydration products in the control cement paste mixture were ettringite and CH; some peaks related to Alite and Belite were also observed, signifying some unreacted cement clinkers. Compared to the reference samples, sludge addition may promote the formation of aluminium-bearing phases, such as $Ca_4Al_2O_7{\cdot}xH_2O$ with the reflection at 10.8° (2θ) and the strätlingite (C_2ASH_8) localised at 21.1° (2θ) and 38.1° (2θ). Also, the peaks related to crystalline ettringite in BP-30 were more evident than those in BP-0. The peak intensity of CH decreased with increasing sludge content, confirming the pozzolanic reactivity of sludge, and these results were corroborated by thermal analysis.

Table 5 Mass loss of mortar samples after corrosion

Mix	Initial mass (g)	Test mass (g)	Mass loss (%)
M-0	133.88	131.38	1.87
M-10	140.08	139.48	0.43
M-20	135.74	132.69	2.25
M-30	138.41	134.48	2.84

Microbiological corrosion durability of mortar samples

The mass loss of the mortar under MIC is given in Table 5. After 2-month corrosion, the mortars containing 10% sludge had a mass loss of 0.43%, significantly lower than the reference (1.87%), exhibiting a stronger resistance to MIC. However, further increasing sludge content did not improve the resistance and even resulted in more severe corrosion than the reference.

The corrosion depth is shown in Fig. 8. The results were consistent with the mass loss. A 10% sludge content reduced the acid penetration in the mortar. The average corrosion depth of M-10 was 2.2 mm (given in Table S3), which was 76% of the reference. However, more than 10% sludge content increased the corrosion rate of mortars. For the samples containing 20% and 30% sludge, the corrosion depth was 117% and 138% of the reference, respectively. These results were confirmed in SEM images, where the dashed line indicated the corrosion interface (see Fig. 9). The obvious gypsum layer

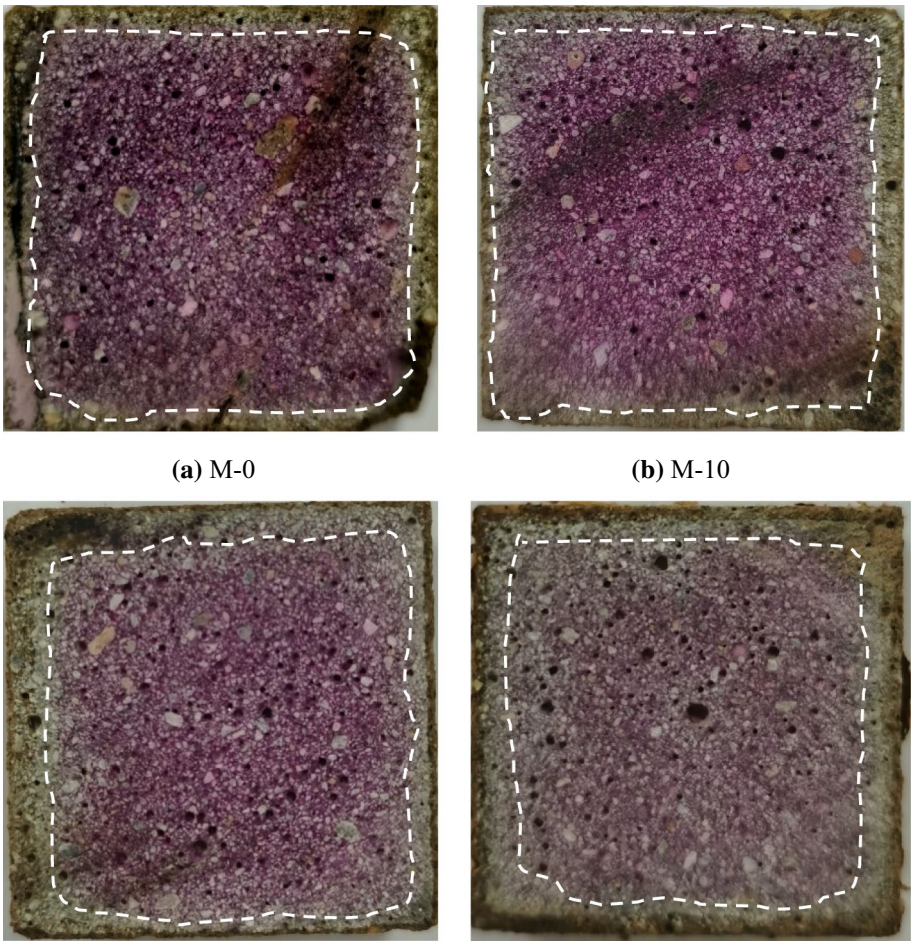

(a) M-0 **(b)** M-10

(c) M-20 **(d)** M-30

Fig. 8 Corrosion depth of mortar with different sludge content. (**a**) M-0, (**b**) M-10, (**c**) M-20, (**d**) M-30

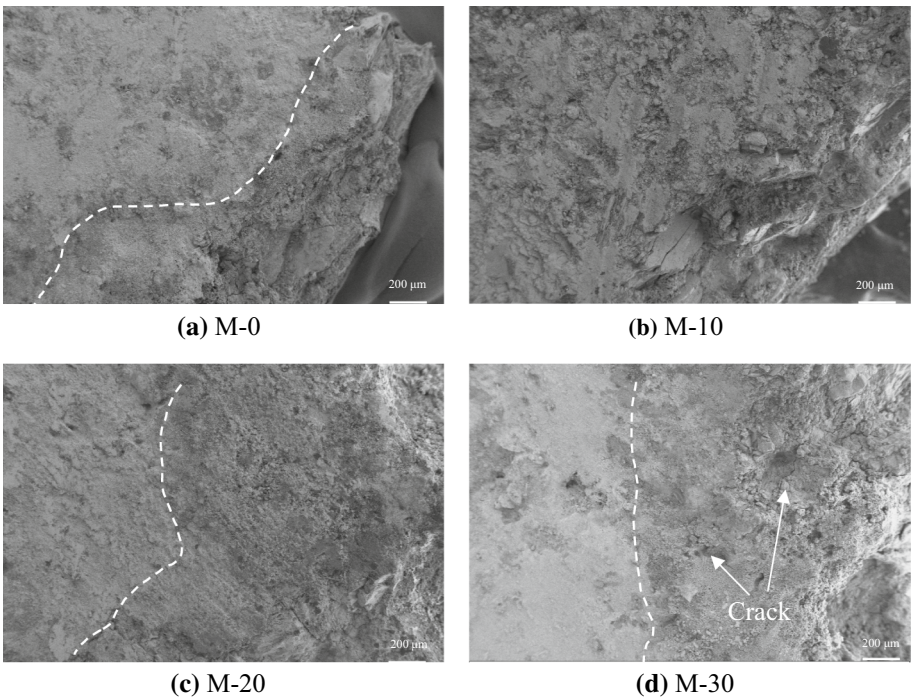

(a) M-0 **(b)** M-10

(c) M-20 **(d)** M-30

Fig. 9 SEM image of corrosion interface. (**a**) M-0, (**b**) M-10, (**c**) M-20, (**d**) M-30

was formed on the surface of M-20 and M-30. In contrast, no clear corrosion interface was observed in M-10. Therefore, according to the mass loss and corrosion depth results, 10% is the optimal sludge proportion in mortars for resisting MIC.

The improved resistance to MIC could be attributed to the high aluminium content in sludge. According to the XRD analysis, more Al-bearing hydrates were formed with increasing sludge proportion in mortar samples, which was beneficial to acid resistance. XRD analysis confirmed the formation of strätlingite from the pozzolanic reaction, which has a stronger acid resistance than C–S–H due to its aluminosilicates framework (Si–O–Al) [39]. On the other hand, the higher water capillary absorption of mortars containing 20% and 30% of sludge indicated a higher mass transportation ability, which could increase the corrosive medium transportation in the mortar matrix, thus accelerating the corrosion rate. The higher sorptivity of the mortars may overcome the positive effect from the Al-bearing hydrates, resulting in more severe corrosion.

Conclusions

Using sludge to replace cement significantly altered the microstructural characteristics of the binder materials and affected the basic properties of sludge-derived mortars. Based on the obtained experimental results, the following conclusions can be drawn:

- Sludge calcined at 800 °C showed the optimum pozzolanic activity, and calcined sludge conformed to the requirements of natural pozzolan materials. The filler effect of sludge accelerated the hydration reaction at early curing ages. With further hydration, the pozzolanic reaction was identified at 28 d and 90 d.
- Ettringite, $Ca_4Al_2O_7{\cdot}xH_2O$, and strätlingite were the main crystalline phases produced during the pozzolanic reaction of sludge. SEM analysis also revealed the existence of laminar products that corresponded to the $Ca_4Al_2O_7{\cdot}xH_2O$ and strätlingite.
- After the MIC test, the mass loss and corrosion depth of the mortar containing 10% sludge were significantly lower than those of the reference sample, and no clear corrosion interface was observed. The improved MIC resistance could be attributed to the additional Al-bearing phases. Further increasing sludge content resulted in more severe corrosion due to increased sorptivity.

Supplementary Information The online version contains supplementary material available at https://doi.org/10.1007/s42768-022-00113-3.

Acknowledgements This research was funded by ARC Research Hub for Nanoscience-based Construction Material Manufacturing, Grant No. IH150100006, General Project of National Natural Science Foundation of China (No. 51778523), and SA Water for the research scholarship and financial support for this project. The authors would like to thank Adelaide Brighton Cement for the supply of cement.

Author contributions Qiong Jia: Data curation, Formal analysis, Investigation, Methodology, Validation, Writing—original draft. Yan Zhuge: Conceptualisation, Methodology, Project administration, Supervision, Writing—review and editing. Weiwei Duan: Formal analysis, Writing—review and editing. Yue Liu: Formal analysis, Writing—review and editing. Jing Yang: Writing—review and editing. Osama Youssf: Writing—review and editing. Jinsuo Lu: Supervision, Writing—review and editing.

Funding Open Access funding enabled and organized by CAUL and its Member Institutions.

Declarations

Conflict of interest The authors declare that they have no known competing financial interests or personal relationships that could have appeared to influence the work reported in this paper. The authors declare the following financial interests/personal relationships which may be considered as potential competing interests:

References

1. Wei, H., Gao, B., Ren, J., et al. 2018. Coagulation/flocculation in dewatering of sludge: A review. *Water Research* 143: 608–631 (**Epub 2018/07/22**).
2. Ren, J., Wang, X., Li, D., et al. 2021. Temperature adaptive microcapsules for self-healing cementitious materials. *Composites Part B: Engineering* 223: 109138.
3. Liu, Y., Zhuge, Y., Chow, C.W.K., et al. 2020. Recycling drinking water treatment sludge into eco-concrete blocks with CO_2 curing: durability and leachability. *Science of The Total Environment* 746: 141182.
4. Li, D., Zhuge, Y., Liu, Y., et al. 2021. Reuse of drinking water treatment sludge in mortar as substitutions of both fly ash and sand based on two treatment methods. *Construction and Building Materials* 277: 122330.
5. Liu, Y., Zhuge, Y., Chow, C.W.K., et al. 2020. Properties and microstructure of concrete blocks incorporating drinking water treatment sludge exposed to early-age carbonation curing. *Journal of Cleaner Production* 261: 121257.
6. Exley, C. 2017. Aluminum should now be considered a primary etiological factor in Alzheimer's disease. *Journal of Alzheimer's Disease Reports* 1: 23.
7. Gibbons, M.K., Mortula, M.M., and Gagnon, G.A. 2009. Phosphorus adsorption on water treatment residual solids. *Journal of Water Supply: Research and Technology—AQUA* 58: 1–10.

8. Ahmad, T., Ahmad, K., and Alam, M. 2016. Sustainable management of water treatment sludge through 3'R' concept. *Journal of Cleaner Production* 124: 1–13.
9. Monteiro, P.J.M., Miller, S.A., and Horvath, A. 2017. Towards sustainable concrete. *Nature Materials* 16: 698–699 (**Epub 2017/06/28**).
10. Gastaldini, A.L.G., Hengen, M.F., Gastaldini, M.C.C., et al. 2015. The use of water treatment plant sludge ash as a mineral addition. *Construction and Building Materials* 94: 513–520.
11. Tantawy, M.A. 2015. Characterization and pozzolanic properties of calcined alum sludge. *Materials Research Bulletin* 61: 415–421.
12. Hagemann, S.E., Gastaldini, A.L.G., Cocco, M., et al. 2019. Synergic effects of the substitution of Portland cement for water treatment plant sludge ash and ground limestone: Technical and economic evaluation. *Journal of Cleaner Production* 214: 916–926.
13. Wu, M., Wang, T., Wu, K., et al. 2020. Microbiologically induced corrosion of concrete in sewer structures: A review of the mechanisms and phenomena. *Construction and Building Materials* 239: 117813.
14. Grengg, C., Mittermayr, F., Baldermann, A., et al. 2015. Microbiologically induced concrete corrosion: A case study from a combined sewer network. *Cement and Concrete Research* 77: 16–25.
15. Mittermayr, F., Rezvani, M., Baldermann, A., et al. 2015. Sulfate resistance of cement-reduced eco-friendly concretes. *Cement and Concrete Composites* 55: 364–373.
16. Scrivener, K., and Capmas, A. 2003. Calcium aluminate cements. *Advanced Concrete Technology* 3: 1–31.
17. Saucier, F., Herisson, J., and Guinot, D. 2018. Use of calcium aluminate cements in sewer networks submitted to H_2S biogenic corrosion. In *Concrete in extreme environments*. Dunbeath: Whittles Publishing.
18. Liu, Y., Zhuge, Y., Chow, C.W., et al. 2022. Effect of alum sludge ash on the high-temperature resistance of mortar. *Resources, Conservation & Recycling* 176: 105958.
19. Frias, M., de la Villa, R.V., García, R., et al. 2013. Mineralogical evolution of Kaolin-based drinking water treatment waste for use as pozzolanic material. The effect of activation Temperature. *Journal of the American Ceramic Society* 96: 3188–3195.
20. Standards Australia. 2010. AS 3972-2010. General purpose and blended cements. Sydney, Australia: Standards Australia.
21. ASTM International. 2013. ASTM D7348-13. Standard test methods for loss on ignition (LOI) of solid combustion residues. West Conshohocken, PA, USA: ASTM International.
22. Standards Australia. 2000. AS 1141.5-2000. Particle density and water absorption of fine aggregate. Sydney, Australia: Standards Australia.
23. ASTM International. 2018. ASTM-C311. Standard test methods for sampling and testing fly ash or natural pozzolans for use in Portland-cement concrete. West Conshohocken, PA: ASTM International.
24. BSI. 2011. BS EN 196-5. Methods of testing cement Part 5: Pozzolanicity test for pozzolanic cement. London, UK: BRITISH STANDARD.
25. ASTM International. 2020. ASTM C305. Standard practice for mechanical mixing of hydraulic cement pastes and mortars of plastic consistency. West Conshohocken, PA: ASTM International.
26. Liu, Y., Zhuge, Y., Chow, C.W.K., et al. 2021. The potential use of drinking water sludge ash as supplementary cementitious material in the manufacture of concrete blocks. *Resources, Conservation and Recycling* 168: 105291.
27. BSI. 2009. BS EN 196-3. Methods of testing cement Part 3: Determination of setting times and soundness. London, UK: BRITISH STANDARD.
28. BSI. 2007. BS EN 1015-3. Methods of test for mortar for masonry Part 3: Determination of consistence of fresh mortar (by flow table). London, UK: BRITISH STANDARD.
29. Standards Australia. 2014. AS 1012.9. Compressive strength tests—Concrete, mortar and grout specimens. Sydney, Australia: Standards Australia.
30. ASTM International. 2013. ASTM C1585. Measurement of rate of absorption of water by hydraulic-cement concretes. West Conshohocken, PA, USA: ASTM International.
31. Fabbri, B., Gualtieri, S., and Leonardi, C. 2013. Modifications induced by the thermal treatment of kaolin and determination of reactivity of metakaolin. *Applied Clay Science* 73: 2–10.
32. ASTM International. 2019. ASTM C618. Standard specification for coal fly ash and raw or calcined natural pozzolan for use in concrete. West Conshohocken, PA, USA: ASTM International.
33. Donatello, S., Tyrer, M., and Cheeseman, C.R. 2010. Comparison of test methods to assess pozzolanic activity. *Cement and Concrete Composites* 32: 121–127.
34. Shi, Y., Matsui, I., and Feng, N. 2002. Effect of compound mineral powders on workability and rheological property of HPC. *Cement and Concrete Research* 32: 71–78.
35. Antoni, M., Rossen, J., Martirena, F., et al. 2012. Cement substitution by a combination of metakaolin and limestone. *Cement and Concrete Research* 42: 1579–1589.
36. Fusade, L., Viles, H., Wood, C., et al. 2019. The effect of wood ash on the properties and durability of lime mortar for repointing damp historic buildings. *Construction and Building Materials* 212: 500–513.
37. Sakai, E., Miyahara, S., Ohsawa, S., et al. 2005. Hydration of fly ash cement. *Cement and Concrete Research* 35: 1135–1140.
38. Gengying, L., and Xiaohua, Z. 2003. Properties of concrete incorporating fly ash and ground granulated blast-furnace slag. *Cement and Concrete Composites* 25: 293–299.
39. Allahverdi, A., and Skvara, F. 2001. Nitric acid attack on hardened paste of geopolymeric cements. Part 1. *Ceramics (Praha)* 45: 81–88.